Development of Time-Integrated Multipoint Moment Analysis for Spatially Resolved Fluctuation Spectroscopy with High Time Resolution

Doogie Oh,[†‡§] Alexandra Zidovska,[†¶‖] Yangqing Xu,[‖] and Daniel J. Needleman[†‡§*]

[†]School of Engineering and Applied Sciences, [‡]Department of Molecular and Cellular Biology, [§]FAS Center for Systems Biology, and [¶]Department of Physics, Harvard University, Cambridge, Massachusetts; and [‖]Department of Systems Biology, Harvard Medical School, Boston, Massachusetts

ABSTRACT Spatial gradients in the behaviors of soluble proteins are thought to underlie many phenomena in cell and developmental biology, but the nature and even the existence of these gradients are often unclear because few techniques can adequately characterize them. Methods with sufficient temporal resolution to study the dynamics of diffusing molecules can only sample relatively small regions, whereas methods that are capable of imaging larger areas cannot probe fast timescales. To overcome these limitations, we developed and implemented time-integrated multipoint moment analysis (TIMMA), a form of fluorescence fluctuation spectroscopy that is capable of probing timescales down to 20 μs at hundreds of different locations simultaneously in a sample. We show that TIMMA can be used to measure the diffusion of small-molecule dyes and fluorescent colloids, and that it can create spatial maps of the behavior of soluble fluorescent proteins throughout mammalian tissue culture cells. We also demonstrate that TIMMA can characterize internal gradients in the diffusion of freely moving proteins in single cells.

INTRODUCTION

The spatial regulation of signaling controls a variety of biological phenomena (1) ranging from the self-organization of subcellular structure (2) to embryonic development (3). Many of these patterns are thought to form from a combination of protein activities, interactions, and diffusion, but few such processes have been analyzed in detail. One difficulty is a lack of tools for studying the spatial regulation of soluble proteins, which are thought to underlie many of these phenomena. Fluorescence resonance energy transfer (FRET) is the most widely used method for measuring spatial variations in protein interactions, but it is difficult to obtain quantitative data with this technique, and it does not provide information on diffusion. Fluorescence fluctuation spectroscopy (FFS) is a powerful collection of methods that are capable of quantitatively measuring the concentrations, diffusion coefficients, and binding constants of soluble molecules in vivo (4). The most frequently used form of FFS is fluorescence correlation spectroscopy (FCS), in which the autocorrelation function of the fluorescence fluctuations is calculated and analyzed. FFS experiments are typically performed with point detectors, with the resulting limitation that the system is only probed at a single diffraction-limited spot at a time. Therefore, although FFS can provide relevant quantitative information about the behaviors of diffusing proteins, it is difficult to use this method to characterize the spatial variations in these behaviors, which are thought to be crucial for biological pattern formation.

A variety of methods have been developed to increase the number of spatial locations that can be probed with FFS. The conceptually simplest approach is to employ multiple point detectors (5–7), but it is impractical to probe a large number of locations with this method due to the difficulty of aligning the system. Another method is to use a single point detector and repetitively scan the observation volume over the sample (8,9), but this approach is limited to studying relatively closely spaced locations because of the time it takes to complete a scan cycle. Recently, a number of groups have used electron-multiplying charge-coupled devices (EMCCDs) as detectors for FCS-style measurements (10–14). EMCCDs are true area detectors with thousands to millions of pixels, so they can be used to simultaneously probe a massive number of locations. However, even the fastest EMCCDs take ~2 ms to acquire an image when the entire detector is used at full resolution. This speed is far too slow to access timescales of tens of microseconds, which are necessary to study freely diffusing small molecules in aqueous solution. One can achieve faster readout of EMCCDs by limiting the area of interest, binning pixels, and using alternative acquisition modes. It is possible to obtain a time resolution of 20 μs if only a single line of pixels is used (11), but this effectively reduces the EMCCD to a line detector instead of an area detector, which makes it difficult to characterize larger systems such as mammalian cells.

Here we describe time-integrated multipoint moment analysis (TIMMA), a method that allows an EMCCD to be used in FFS experiments with a time resolution down to 20 μs while employing up to half the area of the detector. Our approach makes use of the time-integrated cumulant analysis (TICA) formalism developed by Müller and

Submitted February 15, 2011, and accepted for publication August 9, 2011.

*Correspondence: dan_needleman@harvard.edu

Editor: Petra Schwille.

0006-3495/11/09/1546/9 $2.00

doi: 10.1016/j.bpj.2011.08.013

colleagues (15,16), which was originally used with point detectors. We vary the exposure time of the camera and measure the mean and variance of the signal at each location of interest. The dependence of these first two moments on exposure time contains the same information as the correlation function measured in FCS experiments. However, whereas the fastest timescale that can be probed by a correlation analysis is limited by the readout speed of the EMCCD, the smallest timescale that can be probed with a cumulant analysis is determined by the minimum possible exposure time (~20 μs in our setup) and is unrelated to the readout speed of the detector. TIMMA is a generalization of the number and brightness (N&B) method with an EMCCD, as previously described by Unruh and Gratton (10), which extracts information from measurements of the signal mean and variance at a fixed exposure time. Unruh and Gratton (10) also performed related proof-of-principle experiments in their study.

A number of challenges are associated with the use of an EMCCD for TIMMA. First, multiple well-defined optical volumes must be created. We used a stationary spinning disk confocal microscope, as described previously (17), to simultaneously generate hundreds of points suitable for FFS analysis. Second, the exposure time of the EMCCD must be precisely controlled and light must be prevented from striking the chip while the data are being transferred and read out. We gated the laser light to the sample with an acousto-optic tunable filter (AOTF) and ensured synchronization of the EMCCD by triggering both devices with a high-speed signal generator. Third, EMCCDs are intrinsically noisy detectors (10), and if the noise is not corrected for, it can artificially inflate the measured signal variance. We split the signal to create two identical images on the two halves of the EMCCD and computed the covariance of corresponding mirror points. This procedure removes the contribution of the readout noise to the variance in a manner similar to cross-correlating the output of two APDs, which is commonly used to prevent the afterpulsing of these detectors from contaminating FCS measurements. We used an additional background subtraction technique to remove a slight residual additive noise that was correlated over the entire EMCCD. Fourth, the finite dynamic range of the EMCCD limits the range of exposure times that can be investigated for a given particle brightness and concentration. Therefore, we decreased the gain as necessary to avoid saturating the detector when exposure time increased. At each transition region, we recorded the same exposure time with the higher and lower gains and used this overlap to rescale the measurements to correct for the reduction in apparent brightness. By combining these modifications, we were able to use TIMMA to study a wide variety of samples.

We calibrated our system with a freely diffusing dye, validated it by characterizing fluorescent colloidal particles, and used it to perform hundreds of FFS measurements simultaneously on fluorescent proteins in tissue-culture cells. We employed a microfluidics device to demonstrate that TIMMA can quantify internal gradients in the behavior of soluble proteins in single cells. Finally, we used TIMMA to monitor spatial variations in the concentration and dynamics of a fluorescently labeled signaling protein, Ran.

MATERIALS AND METHODS

Microscope

Experiments were carried out on a Nikon eclipse TE2000-E with an apochromat 60× water immersion objective (1.2 NA) and additional 1.5× magnifying optics. A Yokogawa (Tokyo, Japan) CSU-X1 was used for imaging (in spinning mode) and TIMMA measurements (in stationary mode). The diameter of the pinholes on the disk was 50 μm and their physical spacing was 250 μm. We used a total of 90× magnification, so the spacing between observation volumes in the sample was 2.78 μm. The laser power per illumination spot was typically 10 μW (adjusted for each sample to minimize photobleaching). No additional modifications were needed to use the CSU-X1 in stationary mode. A dual view device (DV2; Photometrics, Tucson, AZ) with a 50/50 beam splitter divided the emitted light into two identical images (for noise removal, see above) in front of a demagnifying optics (×0.38) to increase the field of view, and detected with an EMCCD (DV860; Andor Technology, Belfast, Northern Ireland).

Control of laser and camera for data acquisition

Fluorescence excitation was provided by a 488 nm laser (Cyan Scientific CW Laser 100 mW; Spectra-Physics, Santa Clara, CA) modulated by an AOTF (model 48078-2.5-.55; Gooch and Housego, Somerset, UK) with a response time of 12 μs. The AOTF and EMCCD were synchronized by means of a high-speed digital signal generator (NI PCIe-6535; National Instruments, Austin, TX) to ensure a proper exposure time and prevent light from hitting the EMCCD during the readout stage. We acquired data from all locations simultaneously by taking images of the pinhole array with the spinning disk stationary. The fluorescence intensity from multiple neighboring pixels selected from 3 × 3 pixels was integrated to capture most of the light coming from each observation volume.

We obtained mean and covariance curves by acquiring data with different exposure times, typically 25 logarithmically spaced times. We acquired a series of images for each exposure time using the kinetic mode of the EMCCD. In TICA, the signal/noise ratio of a measurement increases with increasing integration time (16). To decrease acquisition times while maintaining similar errors for all exposure times, we reduced the number of images acquired inversely proportional to the exposure time, ranging from ~1000 images for a 50 μs exposure to ~10 images for a 50 ms exposure time. To prevent saturation, the EMCCD gain was periodically decreased as the exposure time was increased. For each of these transitions between gain levels, we acquired two kinetic series: one with the lower gain and one with the higher gain. We then used this overlap to rescale the mean and covariance curves by matching the mean intensity values taken with different gain levels. We averaged 10–15 individual mean and covariance curves together to obtain the final mean and covariance curves. To prevent changes in camera parameters during an exposure series (10), we performed a dummy scan before each series consisting of 60 acquisitions during which the sample was not exposed to light. A background scan was acquired after each measurement series to correct for the nonstationary camera offset (10). We also corrected for a small residual correlation in multiplicative noise, which was present across the entire EMCCD chip and typically had an amplitude ~30-fold smaller than the covariance measured at a pinhole. After accounting for this correlated multiplicative noise, we found that the covariance between neighboring pinholes was ~100 times smaller than the covariance at a pinhole, indicating that the cross-talk between

pinholes is quite small. The entire acquisition process typically took 2–4 min, during which time the sample was exposed to light for 30–40 s. Fits were performed to Eqs. 3 and 4 with weights given by the error associated with the measurements for each exposure time, determined by the standard deviations (SDs) from multiple scanning. Fits that produced R^2-values below a determined number were deemed to be not reliable, and the resulting fit parameters are not plotted in the maps shown in Fig. 3, *C–E*, Fig. 4, *B* and *C*, and Fig. 5. Custom-written Labview codes (National Instruments) were used for all device control, data acquisition, and data analysis.

Sample preparation

A 1 μM stock solution of Molecular Probes Alexa 488 dye (Invitrogen, Carlsbad, CA) in dimethyl sulfoxide and a polymer microsphere (38 nm diameter; Duke Scientific (Thermo Fisher Scientific), Waltham, MA) were diluted in water to the desired concentrations. These in vitro samples were imaged between a glass slide and a coverslip (No. 1.5) sealed with nail polish. HeLa cells stably expressing EGFP were cultured in Dulbecco's modified Eagle's medium (DMEM; Mediatech, Manassas, VA) with 5% CO_2 at 37°C. The HeLa cells were grown on a 25 mm coverslip and transferred to phenol-red free DMEM 12 h before imaging. A custom-built water-heated stage was used to maintain the temperature of the cells on the microscope during the measurements.

Microfluidic device fabrication

Soft lithography was used to fabricate microfluidics devices in polydimethylsiloxane (PDMS, Sylgard 184 silicone elastomer; Dow Corning, Midland, MI) as described elsewhere (18). Devices were bonded to round coverslips (No. 1.5, diameter = 25 mm). Microfluidics channels were coated with 0.1% fibronectin solution (Sigma-Aldrich, St. Louis, MO) before the cell suspension was injected.

RESULTS AND DISCUSSION

Theory behind fluorescence fluctuation analysis

The analysis of fluorescence fluctuations in TIMMA is based on TICA, which uses the time-integrated cumulants of the fluctuating fluorescence signal to extract information about labeled molecules (15,16). This procedure is conceptually different from that performed in FCS. In FCS, information is extracted by explicitly analyzing the time course of the fluctuating signal. Therefore, the fastest timescale that can be probed is determined by how rapidly the signal can be continuously recorded, which for an EMCCD is limited by the readout speed. In contrast, with a cumulant analysis, the actual time course of the signal is not analyzed. Rather, the sample is probed by measuring how the mean and variance (and possibly higher cumulants) vary with exposure time. Fluctuations due to the dynamics of the sample that occur during an exposure will be manifested by increasing the variance of the signal. The timescale of the fluctuations that are probed is given by the timescale of the exposure, which for an EMCCD is limited by the speed at which the illumination can be shuttered, independently of the readout speed. One must acquire multiple images for each exposure time to obtain an accurate estimate of the cumulants. In this approach, only the cumulants (and not the temporal correlations in between the sequential images) are analyzed.

Here we provide an overview of the relevant equations for measuring fluctuations in the first two cumulants, i.e., the mean and the variance (15,16). A noise-free detector exposed to time-varying light with intensity $I(t)$ for a period of time T produces a signal $S = \int_{-T/2}^{T/2} I(t)dt$. If the statistics of the intensity fluctuation are stationary, then the average signal produced from multiple such measurements is

$$S_{avg}(T) \equiv \langle S \rangle = \left\langle \int_{-T/2}^{T/2} I(t)dt \right\rangle = \langle I \rangle T \tag{1}$$

And the variance of these measurements will be

$$\begin{aligned} S_{\mathrm{var}}(T) \equiv \left\langle (\Delta S)^2 \right\rangle &= \left\langle \int_{-T/2}^{T/2} \int_{-T/2}^{T/2} \Delta I(t_1)\Delta I(t_2)dt_1dt_2 \right\rangle \\ &= \langle I \rangle^2 \int_{-T/2}^{T/2} \int_{-T/2}^{T/2} g(t_1 - t_2)dt_1dt_2, \end{aligned} \tag{2}$$

where $\Delta S = S - \langle S \rangle$, the averages are performed over different instances for the time period, T, and $g(t_1 - t_2) = \langle \Delta I(t_1)\Delta I(t_2) \rangle / \langle I \rangle^2$ is the intensity correlation function that is normally measured in FCS experiments. The form of $g(t_1 - t_2)$ depends on the experimental setup and the behavior of the fluorophores. For particles freely diffusing in three dimensions through a Gaussian observation volume, $g(t_1 - t_2) = 1/N(1 + (t_1 - t_2)/\tau_D)^{-1}(1 + (t_1 - t_2)/r^2\tau_D)^{-1/2}$, where N is the average number of molecules in the observation volume, $r = w_z/w_{xy}$ is the ratio of the observation volume's axial width to its radial width, and $\tau_D = w_{xy}^2/4D$ is the average time it takes a particle to diffuse through the observation volume, which is determined by the particle's diffusion coefficient, D. Using this model for the optical system and fluorophore behavior with Eqs. 1 and 2 gives (15,16)

$$S_{avg}(T) = \lambda N T \tag{3}$$

$$\begin{aligned} S_{var}(T) = 4r\lambda^2\tau_D^2 N_\gamma \Bigg(& r - \sqrt{r^2 + \frac{T}{\tau_D}} - \frac{\left(1 + \frac{T}{\tau_D}\right)}{\sqrt{r^2 - 1}} \\ & \times \ln \left[\frac{1 - r^2 + r\sqrt{r^2 - 1} - \left(r - \sqrt{r^2 - 1}\right)\sqrt{r^2 + \frac{T}{\tau_D}}}{\sqrt{1 + \frac{T}{\tau_D}}} \right] \Bigg), \end{aligned} \tag{4}$$

where λ is the brightness per unit time for an individual molecule and γ is the second moment of the observation

volume. Thus, for an ideal camera, the average signal increases linearly with exposure time, T, with a slope that depends on the number, N, and brightness, λ, of the molecules being observed, whereas the variance increases in a more complex fashion, given by Eq. 4. Equation 4 is derived assuming a 3D Gaussian observation value, which would result in $\gamma = \gamma_G = 1/2\sqrt{2} \approx 0.35$ (19), but the true observation volume contains wider tails (17). This deviation is expected to have a minimal influence on the form of the variance curve (Eq. 4 does accurately describe the data; see below), but it could greatly modify γ. We thus continue to use Eq. 4, but treat γ as an empirical parameter that we measure during a calibration step (see below).

EMCCDs are not ideal detectors. For linear, nonideal detectors, the actual measured signal, S_{ms}, is related to the signal that an ideal detector would exhibit, S, by $S_{ms} = \alpha(t)S + \beta(t)$, where $\alpha(t)$ is the multiplicative noise and $\beta(t)$ is the additive noise. To overcome this noise and extract the desired, uncorrupted signal, S, we use a 50/50 beam splitter to divide the signal onto the two halves of the camera. The multiplicative noise is uncorrelated at distant locations on the EMCCD (10), and we have found that the additive noise has weak correlations across the entire camera. Therefore, by both comparing corresponding pixels on the two halves of the chip and performing background subtractions, one can eliminate the contribution of the detector noise.

For a point located at i, with its mirror image located at j (producing measured signals $S_{i,ms}$ and $S_{j,ms}$), we calculate the desired corrected signal as

$$S_{ij,avg}(T) = \sqrt{\left(\langle S_{i,ms}\rangle - \langle \beta_i\rangle\right)\left(\langle S_{j,ms}\rangle - \langle \beta_j\rangle\right)}$$

$$S_{ij,cov}(T) = \langle \Delta S_{i,ms} \Delta S_{j,ms}\rangle - \langle \Delta\beta_i \Delta\beta_j\rangle,$$

where the background signals β_i and β_j are measured in a separate scan with the camera shutter closed. $S_{ij,avg}(T)$ and $S_{ij,cov}(T)$ can then be fit with Eqs. 3 and 4 to determine the relevant parameters at each location in the sample. In practice, this is accomplished by taking multiple images with a fixed exposure time, T, varying the exposure time, and determining how the averages and covariances depend on exposure time (see Materials and Methods).

Dye and colloid sample analysis

To calibrate the microscope system, one must know three numbers that characterize the optical setup: the width of the observation volume, w_{xy}; the asymmetry of the observation volume, $r = w_z/w_{xy}$,; and the second moment of the observation volume, γ. We use $r = 6$, as previously determined for a similar experimental system using a correlation analysis (17), and we measure w_{xy} and γ using a 50 nM Alexa 488 solution as a standard. Fig. 1 shows the mean,

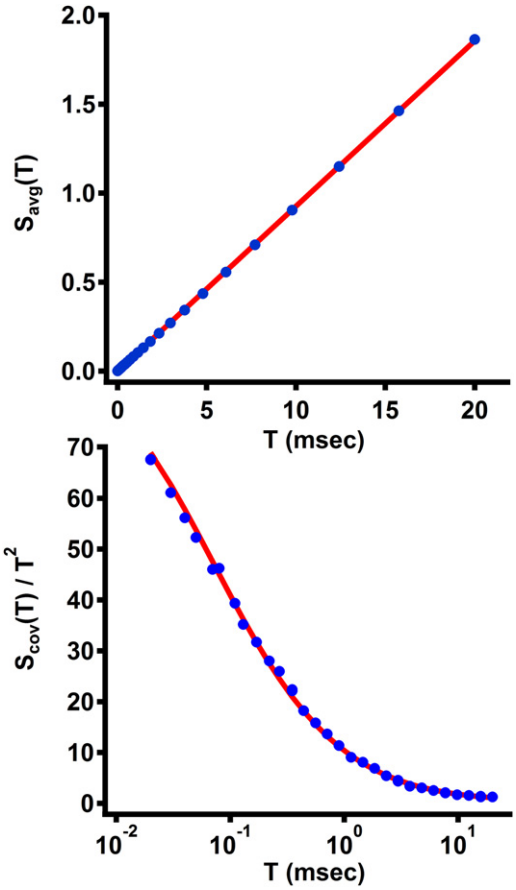

FIGURE 1 Mean and covariance curves of fluorescence intensities of Alexa 488 in aqueous solution as a function of exposure time. Top: Mean curve (*blue dots*) with a best fit to Eq. 3 (*red line*). Bottom: Covariance curve (*blue dots*) with a best fit to Eq. 4 (*red line*).

$S_{avg}(T)$, and covariance, $S_{cov}(T)$, curves for Alexa 488 from $T = 20$ μs to $T = 20$ ms, fit to Eqs. 3 and 4. Using a diffusion coefficient for Alexa 488 of 435 $\mu m^2/s$ (20) and the measured diffusion time of $\tau_D = 22.5 \pm 3.2$ μs gives $w_{xy} = 0.198 \pm 0.020$ μm, which, within error, is equivalent to what was determined for a similar setup with a correlation analysis of slower diffusion particles (17). The known concentration of Alexa 488 (50 nM) allows a fit to Eq. 4 to determine $\gamma = 0.060 \pm 0.090$. This γ is much smaller than expected for a 3D Gaussian, $\gamma_G = 1/2\sqrt{2} \approx 0.35$ (19), which is consistent with the known extended tails of the observation volume in this system (17), and is similar to the value expected for a Gaussian-Lorentzian, $\gamma_{GL} = 3/4\pi^2 \approx 0.078$ (19). These calibration results yield an observation volume of 0.26 ± 0.045 fL. Having calibrated the system by determining w_{xy}, r, and, γ, we can investigate novel systems with TIMMA, fit the mean and covariance curves with Eqs. 3 and 4, and thereby measure the concentration, diffusion coefficient, and brightness of particles.

We first tested the calibrated system using another well-characterized in vitro sample: fluorescent colloids. We

obtained data simultaneously from 50 different locations with exposure times ranging from $T = 20\ \mu s$ to $T = 20$ ms. The mean and variance curves at one location are shown in Fig. 2 *A*, with corresponding fits to Eqs. 3 and 4. Fits were performed for each of the 50 locations (Fig. 2 *B*). The fluorescent colloid sample is homogeneous, so the spread in the fit parameters provides an indication of the precision of the measurement (as the optical properties of the spinning disk pinholes are quite uniform (17)). The SD of each of the fit parameters is <15% of the mean, demonstrating the good reproducibility of the method, with $\lambda = 5.3 \pm 0.75$ AU, a concentration 63.1 ± 7.8 nM, and a diffusion coefficient of 9.8 ± 1.4 $\mu m^2/s$. This measured diffusion coefficient is close to the expected value of 11.6 $\mu m^2/s$, given the manufacturer's specified diameter of 0.038 μm for these colloids. We further validated the system by confirming that changing the concentration of colloids produced a linear change in the measured concentration of colloids, but did not affect the measured diffusion coefficient (Fig. 2 *C*).

Diffusion of EGFP in vivo

We next tested the utility of the system for in vivo measurements by studying the diffusion of EGFP in mammalian tissue-culture cells. We took data from nine cells, with 90–200 observation volumes per cell, to obtain a mean diffusion coefficient (and SD) of 34.7 ± 2.5 $\mu m^2/s$ for EGFP in these cells, which is similar to what has been determined previously (21,22). The field of view that can be investigated in a single measurement is large enough to allow multiple cells to be probed simultaneously. Fig. 3 *A* shows an image of three HeLa cells expressing soluble EGFP taken with the Nipkow disk spinning. The disk was stopped for TIMMA measurements, and mean and covariance curves were obtained for 150 locations covering all three cells. Representative mean and covariance data, with corresponding fits, for two of these locations are shown in Fig. 3 *B*. Similar fits were performed for all locations, which allowed us to create maps of the diffusion, concentration, and brightness of EGFP throughout these cells (Fig. 3, *C–E*). The maps of

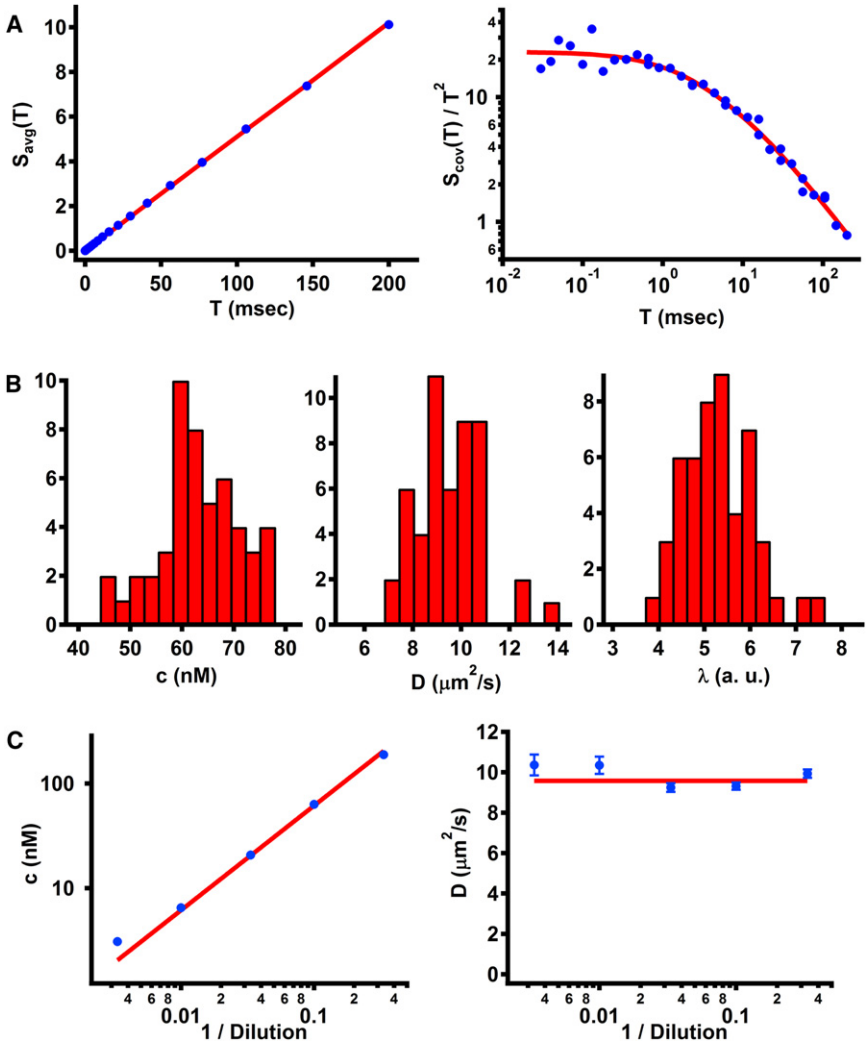

FIGURE 2 Analysis of data obtained with colloid sample. (*A*) Mean and covariance curves from an individual pinhole (*blue dots*) with fits to Eqs. 3 and 4 (*red lines*). (*B*) Histograms of fit parameters from 50 different observation volumes showing the measured concentration, diffusion coefficient, and particle brightness. (*C*) Measured concentration and diffusion coefficient as a function of inverse dilution from the stock solution.

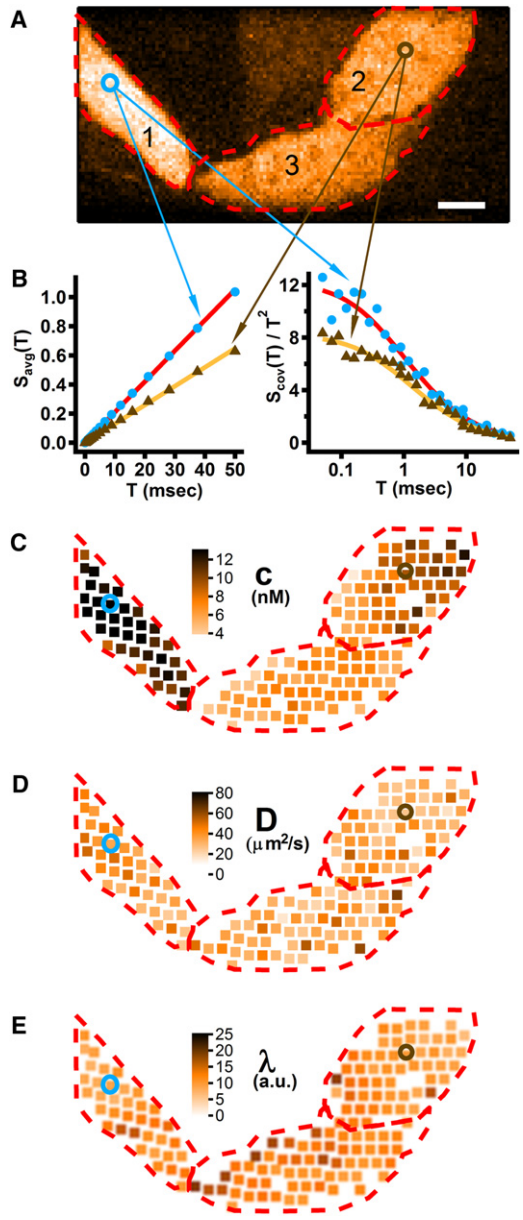

FIGURE 3 Analysis of EGFP diffusion in HeLa cells. (*A*) Image of three HeLa cells taken with spinning-disk confocal in imaging mode. Scale bar: 10 μm. (*B*) Mean and covariance curves with associated fits for two different locations (indicated in *A* and *C–E*): cell 1 and cell 2. (*C*) Map of concentration measured at the each location corresponding to an observation volume. (*D*) Map of diffusion coefficient. (*E*) Map of single fluorophore brightness.

diffusion coefficient (Fig. 3 *D*) and brightness (Fig. 3 *E*) show that these quantities are similar in all three cells, with an average (and SD) across all points of 32.1 ± 10.4 $\mu m^2/s$ and 10.6 ± 2.4 AU. In contrast, the concentration of EGFP in these three cells is significantly different, with one cell having a concentration of (mean and standard error) 12.6 ± 0.3 nM, another cell having 8.0 ± 0.3 nM, and the third cell having 6.4 ± 0.2 nM. Thus, as expected, the differences in brightness among the three cells observed in imaging (Fig. 3 *A*) were caused by the different concentrations of EGFP in these cells, not by any change in the brightness of individual EGFP molecules.

Spatial gradients of soluble proteins in single cells

One of our motivations for developing a system capable of high-speed, multipoint FFS was to study spatial variations in the behaviors of soluble proteins in individual cells, which have been proposed to be important for cell organization and signaling (1). We therefore sought to demonstrate that our method is capable of measuring such internal gradients by studying a simple model system.

As shown above, the diffusion coefficient of EGFP in HeLa cells is spatially homogeneous. This diffusion coefficient is a function of the osmolarity of the media in which the cells are immersed, changing from 34.7 ± 2.5 $\mu m^2/s$ for cells in DMEM (see above) to 18.8 ± 1.6 $\mu m^2/s$ for cells in DMEM with 10% PEG (molecular weight = 400). We used this difference to create cells with internal gradients in the diffusion of EGFP by employing a microfluidics device to expose regions of cells to different osmotic stresses (Fig. 4 *A*). The device contained channels that were 10 μm × 10 μm × 500 μm. Cells were loaded into the microfluidic devices by flow and, after settling for 30 min, they completely occluded the channels. Cells loaded into these microfluidics channels and exposed to buffer without osmolite on both ends exhibited spatially uniform diffusion of EGFP (Fig. 4 *B*). However, if one end of the cell is exposed to buffer with 10% PEG while the other end is exposed to buffer without PEG, an internal gradient of the diffusion of EGFP develops (Fig. 4). The behavior of EGFP varies from point to point due to the complex internal structure of the cell (Fig. 4 *C*). A clear pattern emerges when the average diffusion coefficient is calculated in different regions of the cell (Fig. 4 *D*): the diffusion coefficient gradually increases across the cell. The diffusion coefficient at the rightmost side of the cell partially exposed to PEG is 17.8 ± 2.5 $\mu m^2/s$, similar to the value obtained for cells entirely immersed in 10% PEG, whereas the diffusion coefficient at the leftmost side is 26.7 ± 2.8 $\mu m^2/s$, still somewhat less than obtained for cells solely in DMEM. This result demonstrates that our technique can measure even relatively subtle internal gradients in the behavior of soluble proteins, and thus should be highly useful for studying a variety of problems in cell and developmental biology.

Spatial dynamics of the GTPase Ran in single cells

One of the most promising uses of TIMMA is to characterize spatial variations in the behaviors of biologically relevant fusion proteins in single cells. To demonstrate the capabilities of TIMMA in this regard, we performed

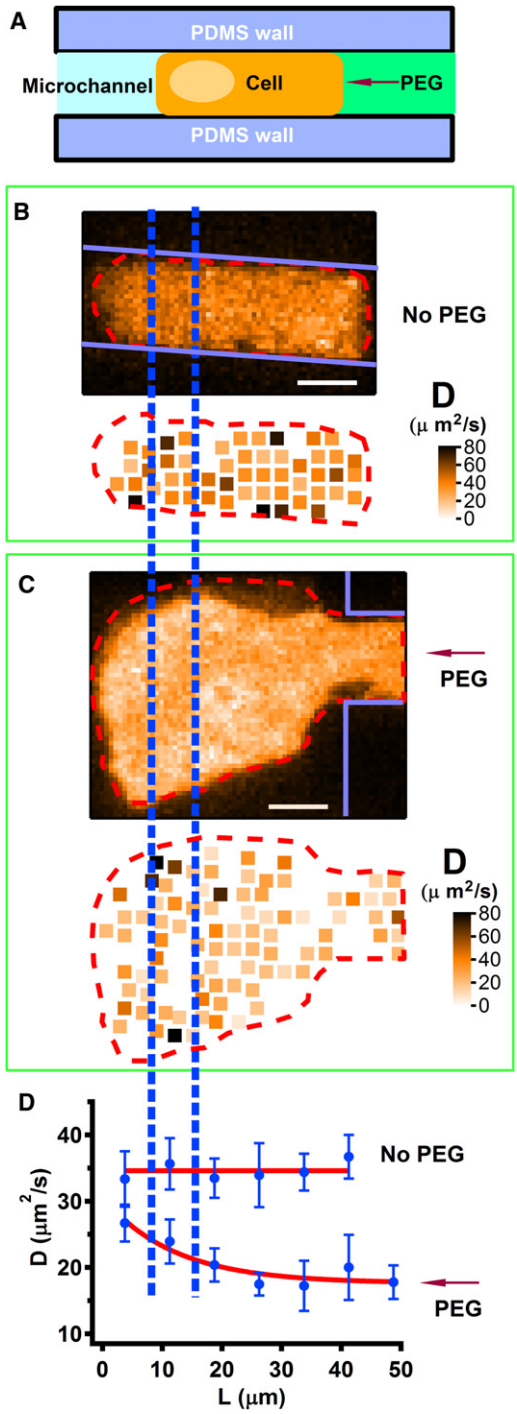

FIGURE 4 Analysis of EGFP diffusion in HeLa cells subjected to an osmotic gradient. (*A*) Schematics of the experimental setup. (*B*) Top: An image of a cell in the microfluidic device without exposure to PEG, with the PDMS walls (*blue lines*) and cell boundary (*red dotted line*) indicated. Bottom: A map of the measurements of EGFP diffusion coefficient at different locations. (*C*) Top: An image of a cell in the microfluidics device exposed to PEG from one end, with the PDMS walls (*blue lines*) and cell boundary (*red dotted line*) indicated. Bottom: A map of the measurements of EGFP diffusion coefficient at different locations. Scale bar: 10 μm. (*D*) The average diffusion coefficient in these two cells as a function of position along the cell. The red lines are guides to the eye.

measurements on U2OS cells transiently expressing EGFP-Ran, a GTPase involved in nuclear import and mitosis (23). Fig. 5 (*top*) shows an image of EGFP-Ran in a cell (*left*), along with spatial maps of the concentration, diffusion coefficient, and brightness. We separately analyzed the behavior of EGFP-Ran in the nucleus and the cytoplasm. In the nucleus, the mean (and standard error) of the concentration of EGFP-Ran was 20.8 $\pm$ 0.8 nM, whereas its diffusion coefficient was 16.5 $\pm$ 1.4 $\mu m^2/s$ and its brightness was 3.8 $\pm$ 0.6 AU. In the cytoplasm, these values were 5.7 $\pm$ 0.4 nM, 24.7 $\pm$ 1.6 $\mu m^2/s$, and 4.1 $\pm$ 0.2 AU, respectively. This approximately fourfold increase in the concentration of Ran in the nucleus, and the uniform molecular brightness of labeled Ran throughout cells, was previously observed with the N&B technique (24), and the decreased mobility of Ran in the nucleus was studied with FCS (24). These results demonstrate that TIMMA can be used to study biologically functional fluorescently tagged proteins.

CONCLUSIONS

In this work, we developed TIMMA, a high-speed, highly parallel form of FFS that is capable of measuring dynamics at timescales down to 20 μs at hundreds of locations simultaneously. We calibrated our system using a freely diffusing small molecule and demonstrated its performance by studying fluorescent colloids. We showed that TIMMA can simultaneously measure the diffusion of EGFP at hundreds of locations in multiple tissue-culture cells, and can even map internal gradients in the behaviors of soluble proteins in single cells. TIMMA makes use of a stationary spinning disk confocal system (17) to generate hundreds of observation volumes, and an EMCCD area detector with an acquisition protocol based on TICA (15,16) to investigate the dynamics of fluctuations at timescales orders of magnitude faster than the readout speed of the camera. Implementation of this method required a number of developments, most significantly procedures to deal with the noise and limited dynamic range of the detector.

TIMMA can access timescales orders of magnitude faster than is possible with conventional correlation analysis with an EMCCD (12,13,17,25), and thus has a clear advantage for studying rapidly diffusing, soluble molecules. Use of the fast kinetic mode of EMCCDs allows similar timescales to be probed (11), but that technique is limited to reading out at most a few rows of pixels. An FCS measurement obtained with an EMCCD in fast kinetic mode typically has an acquisition time of ~1.5 min or longer (11,26,27), which is somewhat more rapid than the 2–4 min acquisition time of TIMMA, but TIMMA can be used to probe an area ~40 times larger in that time frame. In a previous study, Unruh and Gratton (10) used EMCCDs to measure the mean and variance at a fixed exposure time, and thus were able to extract the number and brightness of molecules. TIMMA can be viewed as a generalization of this previous method, called N&B,

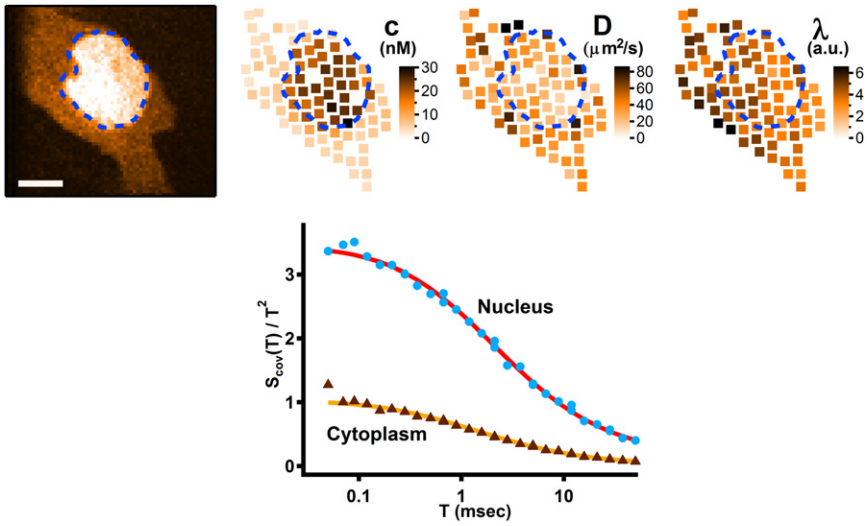

FIGURE 5 Analysis of EGFP-Ran diffusion in U2OS cells. Upper left: Confocal image of an EGFP-Ran-transfected U2OS cell. Scale bar: 10 μm. Top: Three maps of concentration, diffusion coefficient, and brightness are shown (the *dashed blue line* encircles the nucleus). Bottom: Covariance curves from EGFP-Ran in the nucleus and cytoplasm.

with the advantage that it can extract more-detailed information about the dynamics of molecules, but the disadvantage that it requires more-complex experimental setup and data analysis. Typical acquisition times for TIMMA are 2–4 min (during which the sample is exposed to light for ~30–40 s), and in this time period hundreds of locations can be probed in multiple cells. Single point measurements can obtain high-quality data in ~30 s (28); therefore, if <~8 points are being investigated, it takes less time to use sequential point measurements, whereas TIMMA is more rapid for larger number of locations. Repetitive point scanning can extract information from spatial correlations (8) and is less prone to artifacts (9), but such techniques are typically limited to probing spatial scales of a few microns or less, due to the time it takes the scan to complete one cycle.

TIMMA is a powerful new method for studying internal gradients in the behaviors of soluble proteins in cells. A promising future direction would be to develop a two-color version (29) for mapping gradients in protein interactions or to extend the method to higher cumulants (16) to measure homo-oligomerization. It will also be possible to use a similar acquisition protocol with different illumination schemes such as total internal reflection (13) or single-plane illumination microscopy (14), which have advantages for studying very thin and thick samples, respectively.

We thank Philippe Cluzel and Jeff Moffitt for advice and comments on the manuscript, and Paul Clarke (University of Dundee) for the gift of the EGFP-Ran plasmid. We thank Andor Technology for assistance with the software development kit.

This work was supported by National Science Foundation grant 0959721 to D.J.N. A.Z. is a Damon Runyon Fellow supported by the Damon Runyon Cancer Research Foundation (DRG 2040-10).

REFERENCES

1. Kholodenko, B. N. 2006. Cell-signalling dynamics in time and space. *Nat. Rev. Mol. Cell Biol.* 7:165–176.
2. Bastiaens, P., M. Caudron, …, E. Karsenti. 2006. Gradients in the self-organization of the mitotic spindle. *Trends Cell Biol.* 16:125–134.
3. Lander, A. D. 2007. Morpheus unbound: reimagining the morphogen gradient. *Cell.* 128:245–256.
4. Vukojević, V., A. Pramanik, …, G. Bakalkin. 2005. Study of molecular events in cells by fluorescence correlation spectroscopy. *Cell. Mol. Life Sci.* 62:535–550.
5. Brinkmeier, M., K. Dörre, …, M. Eigen. 1999. Two-beam cross-correlation:ca method to characterize transport phenomena in micrometer-sized structures. *Anal. Chem.* 71:609–616.
6. Dittrich, P. S., and P. Schwille. 2002. Spatial two-photon fluorescence cross-correlation spectroscopy for controlling molecular transport in microfluidic structures. *Anal. Chem.* 74:4472–4479.
7. Ohsugi, Y., and M. Kinjo. 2009. Multipoint fluorescence correlation spectroscopy with total internal reflection fluorescence microscope. *J. Biomed. Opt.* 14:014030.
8. Ruan, Q. Q., M. A. Cheng, …, W. W. Mantulin. 2004. Spatial-temporal studies of membrane dynamics: scanning fluorescence correlation spectroscopy (SFCS). *Biophys. J.* 87:1260–1267.
9. Digman, M. A., C. M. Brown, …, E. Gratton. 2005. Measuring fast dynamics in solutions and cells with a laser scanning microscope. *Biophys. J.* 89:1317–1327.
10. Unruh, J. R., and E. Gratton. 2008. Analysis of molecular concentration and brightness from fluorescence fluctuation data with an electron multiplied CCD camera. *Biophys. J.* 95:5385–5398.
11. Burkhardt, M., and P. Schwille. 2006. Electron multiplying CCD based detection for spatially resolved fluorescence correlation spectroscopy. *Opt. Express.* 14:5013–5020.
12. Kannan, B., J. Y. Har, …, T. Wohland. 2006. Electron multiplying charge-coupled device camera based fluorescence correlation spectroscopy. *Anal. Chem.* 78:3444–3451.
13. Kannan, B., L. Guo, …, T. Wohland. 2007. Spatially resolved total internal reflection fluorescence correlation microscopy using an electron multiplying charge-coupled device camera. *Anal. Chem.* 79:4463–4470.
14. Wohland, T., X. K. Shi, …, E. H. Stelzer. 2010. Single plane illumination fluorescence correlation spectroscopy (SPIM-FCS) probes inhomogeneous three-dimensional environments. *Opt. Express.* 18:10627–10641.
15. Müller, J. D. 2004. Cumulant analysis in fluorescence fluctuation spectroscopy. *Biophys. J.* 86:3981–3992.
16. Wu, B., and J. D. Müller. 2005. Time-integrated fluorescence cumulant analysis in fluorescence fluctuation spectroscopy. *Biophys. J.* 89:2721–2735.

17. Needleman, D. J., Y. Q. Xu, and T. J. Mitchison. 2009. Pin-hole array correlation imaging: highly parallel fluorescence correlation spectroscopy. *Biophys. J.* 96:5050–5059.

18. Duffy, D. C., J. C. McDonald, …, G. M. Whitesides. 1998. Rapid prototyping of microfluidic systems in poly(dimethylsiloxane). *Anal. Chem.* 70:4974–4984.

19. Chen, Y., J. D. Müller, …, E. Gratton. 1999. The photon counting histogram in fluorescence fluctuation spectroscopy. *Biophys. J.* 77:553–567.

20. Petrásek, Z., and P. Schwille. 2008. Precise measurement of diffusion coefficients using scanning fluorescence correlation spectroscopy. *Biophys. J.* 94:1437–1448.

21. Kim, S. A., and P. Schwille. 2003. Intracellular applications of fluorescence correlation spectroscopy: prospects for neuroscience. *Curr. Opin. Neurobiol.* 13:583–590.

22. Dragestein, K. A., W. A. van Cappellen, …, N. Galjart. 2008. Dynamic behavior of GFP-CLIP-170 reveals fast protein turnover on microtubule plus ends. *J. Cell Biol.* 180:729–737.

23. Weis, K. 2003. Regulating access to the genome: nucleocytoplasmic transport throughout the cell cycle. *Cell.* 112:441–451.

24. Abu-Arish, A., P. Kalab, …, C. Fradin. 2009. Spatial distribution and mobility of the Ran GTPase in live interphase cells. *Biophys. J.* 97:2164–2178.

25. Kolin, D. L., and P. W. Wiseman. 2007. Advances in image correlation spectroscopy: measuring number densities, aggregation states, and dynamics of fluorescently labeled macromolecules in cells. *Cell Biochem. Biophys.* 49:141–164.

26. Heuvelman, G., F. Erdel, …, K. Rippe. 2009. Analysis of protein mobilities and interactions in living cells by multifocal fluorescence fluctuation microscopy. *Eur. Biophys. J.* 38:813–828.

27. Yu, S. R., M. Burkhardt, …, M. Brand. 2009. Fgf8 morphogen gradient forms by a source-sink mechanism with freely diffusing molecules. *Nature.* 461:533–536.

28. Kim, S. A., K. G. Heinze, and P. Schwille. 2007. Fluorescence correlation spectroscopy in living cells. *Nat. Methods.* 4:963–973.

29. Schwille, P., F. J. Meyer-Almes, and R. Rigler. 1997. Dual-color fluorescence cross-correlation spectroscopy for multicomponent diffusional analysis in solution. *Biophys. J.* 72:1878–1886.